1 of 9



Received: 9 February 2023 Revised: 10 March 2023 Accepted: 24 March 2023

# Electrochemical performance and impedance of a conical pore in the low–Pt PEM fuel cell catalyst layer

# Andrei Kulikovsky D

Research Computing Center, Lomonosov Moscow State University, Moscow, Russia

#### Correspondence

Andrei Kulikovsky, Research Computing Center, Lomonosov Moscow State University, Moscow, Russia Email: A.Kulikovsky@fz-juelich.de

#### Present address

Andrei Kulikovsky, Forschungszentrum Jülich GmbH, Theory and Computation of Energy Materials (IEK13), Institute of Energy and Climate Research, Jülich, Germany

#### **Abstract**

A model for the transient electrochemical performance of a conical pore in the cathode catalyst layer of a low–Pt PEM fuel cell is developed. The pore is separated from the Pt surface by a thin ionomer film. A transient equation for the oxygen diffusion along the pore coupled to the proton conservation equation in the ionomer film is derived. Numerical solution of the static equations shows superior electrochemical performance of a conical pore as compared to cylindrical pore with equivalent electrochemically active surface area. Equations for the pore impedance are derived by linearization and Fourier–transform of transient equations. The conical pore impedance is calculated and compared to the impedance of equivalent cylindrical pore. It is shown that the pore shape affects the frequency dependence of impedance.

#### KEYWORDS

impedance, low Pt loading, modeling, PEM fuel cell

### 1 | INTRODUCTION

Cathode catalyst layer (CCL) is a key component of polymer electrolyte fuel cells. In this layer, oxygen meets protons and electrons to convert the charged species into water. To maximize catalyst surface area for the oxygen reduction reaction (ORR), the CCL is designed as a porous media comprising of three interpenetrating clusters of Pt/C particles, ionomer for proton transport and void pores for oxygen transport.

Understanding and engineering optimal CCL is a key problem in PEMFC technology (see recent reviews <sup>[1,2]</sup>). A vast majority of research papers are focused on randomly structured CCLs produced by hot–pressing ionomer ink with dissolved Pt/C particles onto a membrane. Basic CCL design parameters are catalyst particles structure/composition, ionomer to carbon ratio and pore size distribution <sup>[1,3,4]</sup>. These parameters need to be opti-

mized to satisfy contradictory requirements: for example, good oxygen transport requires lowering of ionomer content to provide more open space for gaseous diffusion, while better proton transport requires increasing the ionomer content.

Increasing the performance of a low-Pt PEMFC is a problem of tremendous importance for the technology. Solution of this problem would help to reduce the cost of PEMFC-based power sources. Any hints from the modeling side helping to improve performance of a low-Pt cell are of interest for the fuel cell community.

Models of low–Pt catalyst layer performance have been focused on oxygen transport though a single Pt/C agglomerate surrounded by a thin ionomer film <sup>[5–11]</sup>. The rate of oxygen conversion in the agglomerate is calculated taking into account details of Pt/C particles and ionomer film structure. This rate is then substituted into standard macro–homogeneous model for oxygen and proton

This is an open access article under the terms of the Creative Commons Attribution License, which permits use, distribution and reproduction in any medium, provided the original work is properly cited.

 $@\ 2023\ The\ Authors.\ \textit{Electrochemical Science Advances}\ published\ by\ Wiley-VCH\ GmbH.$ 

fülich GmbH Research Center, Wiley Online Library on [23/08/2024]. See the Terms

use; OA articles are governed by the applicable Creative Commons L

transport through the CCL depth to calculate the CCL polarization curve. In this way, parametric dependencies of the cell polarization curve on agglomerate structure have been studied. However, these models describe oxygen transport through the CCL only in a mean–field manner, not specifying geometry of the void pores.

On experimental side, a novel technology of using scalable nanoporous carbon films with tunable pore size and shape for CCL production has been reported <sup>[12]</sup>. Ultrathin carbon nanotube-based CCLs exhibiting excellent performance and durability have been demonstrated <sup>[13]</sup>; however, these materials are not widely spread seemingly due to their high cost. These works indicate interest of research community in regularly structured catalyst layers.

In this paper, a transient model for electrochemical performance of a conical nanopore is developed. Pores in the CCL are surrounded by Pt/C agglomerates covered by a thin ionomer film. To model this structure, conical pore is separated from the coaxial Pt/C tube by an ionomer film. In low-Pt PEMFCs, ionomer film provides a significant barrier to oxygen transport at high currents [14]. The model, thus, includes the main features of a low-Pt CCL: oxygen transport along the void pore, oxygen dissolution in the ionomer, proton transport in the ionomer, and ORR at the ionomer/Pt interface. The model is extension of the model for cylindrical pore performance and impedance which helped to understand the effect of oxygen transport through Nafion film on the low-Pt cell polarization curve and spectra [15,16]. Here we show that the conical pore converging toward the membrane exhibits much better performance as compared to cylindrical pore with equivalent active surface area.

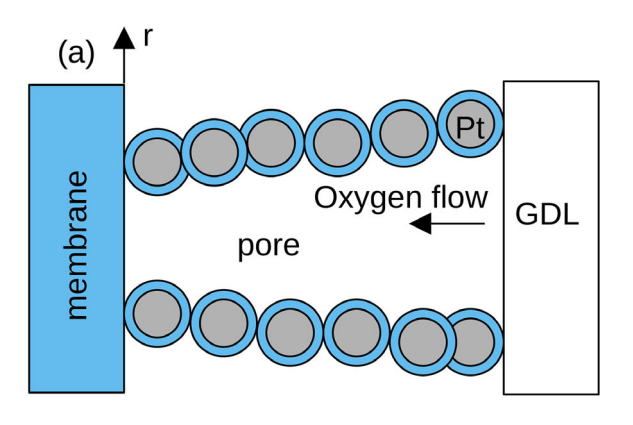
Similar problem of oxygen transport in a water-filled conical nanopore has been considered in <sup>[17]</sup>. The authors solved numerically a two-dimensional oxygen transport equation in the nanopore. Here we demonstrate that the problem can be reduced to one-dimensional one, which greatly simplifies the numerical solution.

Further, linearization and Fourier-transform of the transient mass and charge conservation equations give linear equations for the perturbation amplitudes. A fast method for numerical solution of the system of linear ODEs is suggested; using this method, impedance of conical and cylindrical pores are calculated and compared.

#### 2 | MODEL

The model is constructed under the following general assumptions:

1. The cell is isothermal.



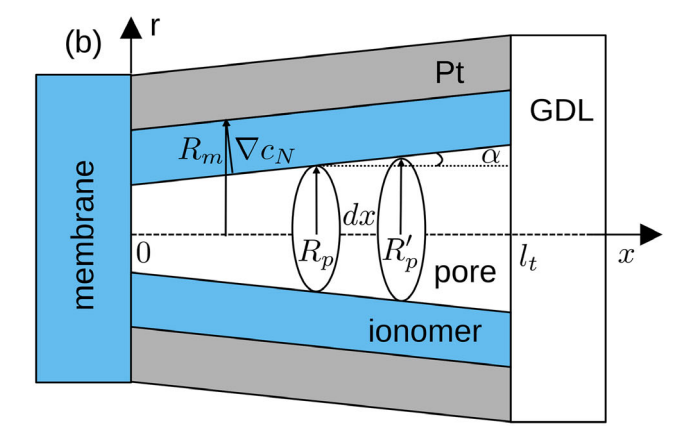


FIGURE 1 (a) Schematic of a conical pore formed by P/C agglomerates covered by a thin ionomer film. (b) A model for the conical pore performance and the system of coordinates.

- The stoichiometry of air flow is large and the oxygen concentration and current density are uniform over the cell active area.
- 3. The oxygen transport in the gas-diffusion layer (GDL) is ignored. This transport could be easily incorporated by changing the boundary conditions for the oxygen concentration and flux at the CCL/GDL interface.
- 4. The CCL flooding effects are not considered in this work.

# 2.1 | Equation for oxygen transport in a conical pore

Schematic of a single conical pore is shown in Figure 1. Oxygen is transported along the pore from the GDL toward the membrane. Consider a small pore volume element of a thickness dx (Figure 1b). The element has a form of conoid with the small and large bases formed by the circles of the radii  $R_p$  and  $R_p' = R_p + dx \tan \alpha$ , where  $\alpha$  is the conoid half–angle (Figure 1b).

Chemistry Europe

European Chemical Societies Publishing

The balance of oxygen fluxes in the volume element is

$$\pi (R_p + dx \tan \alpha)^2 D_{ox} \frac{\partial c}{\partial x} \Big|_{x+dx} - \pi R_p^2 D_{ox} \frac{\partial c}{\partial x} \Big|_x$$

$$= \pi (R_p + R_p + dx \tan \alpha) dx \frac{N_p}{\cos \alpha}$$
 (1)

where c is the oxygen concentration,  $D_{ox}$  is the oxygen diffusion coefficient in a void pore space, and

$$N_p = -D_N \frac{\partial c_N}{\partial r} \Big|_{r=R_n+} \tag{2}$$

is the radial diffusive flux of oxygen dissolved in the ionomer (see below).

Dividing both sides of Equation (1) by  $\pi R_p^2 dx$  and setting  $dx \to 0$ , we come to

$$D_{ox}\frac{\partial^2 c}{\partial x^2} + \frac{2\tan(\alpha)}{R_p}D_{ox}\frac{\partial c}{\partial x} = \frac{2N_p}{R_p\cos\alpha}$$
 (3)

It is convenient to introduce dimensionless variables

$$\tilde{x} = \frac{x}{l_t}, \quad \tilde{r} = \frac{r}{l_t}, \quad \tilde{t} = \frac{ti_*}{C_{dl}b} \quad \tilde{c} = \frac{c}{c_{h}^{in}}, \quad \tilde{j} = \frac{jl_t}{\sigma_N b},$$

$$\tilde{\eta} = \frac{\eta}{b}, \quad \tilde{D}_{ox} = \frac{4FD_{ox}c_h^{in}}{\sigma_N b}, \quad \tilde{N}_p = \frac{4Fl_tN_p}{\sigma_N b},$$

$$\tilde{Z} = \frac{Z\sigma_N}{l_t}, \quad \tilde{\omega} = \frac{\omega C_{dl}b}{l_*} \quad (4)$$

where  $l_t$  is the pore length,  $c_h^{in}$  is the reference (inlet) oxygen concentration,  $\sigma_N$  is the ionomer film proton conductivity, b is the ORR Tafel slope, j is the local proton current density,  $\eta$  is the cathode overpotential, positive by convention,  $C_{dl}$  is the double layer volumetric capacitance,  $i_*$  is the ORR volumetric exchange current density, Z is the impedance, and  $\omega$  is the angular frequency (see below).

With the dimensionless variables, Equation (3) takes the form

$$\varepsilon^2 \tilde{D}_{ox} \left( \frac{\partial^2 \tilde{c}}{\partial \tilde{x}^2} + \frac{2 \tan(\alpha)}{\tilde{R}_p(\tilde{x})} \frac{\partial \tilde{c}}{\partial \tilde{x}} \right) = \frac{2\varepsilon^2 \tilde{N}_p}{\tilde{R}_p(\tilde{x}) \cos \alpha}$$
 (5)

where  $\varepsilon$  is the dimensionless Newman's reaction penetration depth

$$\varepsilon = \sqrt{\frac{\sigma_N b}{i_* l_t^2}} \tag{6}$$

$$\tilde{R}_p(\tilde{x}) = \tilde{R}_{p,0} + \tilde{x} \tan(\alpha), \tag{7}$$

and  $\tilde{R}_{p,0}$  is the pore radius at the membrane surface ( $\tilde{x} = 0$ ). Note that  $\alpha > 0$  describes a divergent toward the GDL pore shape, as in Figure 1, and  $\alpha < 0$  corresponds to a convergent shape.

It is important to note that any axially symmetric pore of an arbitrary smooth shape can be approximated by a set of conical rings of infinitesimal thickness. This means that Equation (5) describes diffusive transport in a pore with any curved side surface, provided that the pore radius  $\tilde{R}_p(\tilde{x})$  is given as a continuous function of  $\tilde{x}$ . The tanfunction of the pore surface generatrix slope is given by  $\tan(\alpha(\tilde{x})) = \partial \tilde{R}_p/\partial \tilde{x}$ .

# 2.2 $\mid$ Proton and oxygen transport in the ionomer film

Protons move in the ionomer film along the coordinate x (field direction). It is assumed that the Pt/C conoid has openings through which protons can reach the ionomer film/Pt interface from the outside of the Pt/C cone. Assuming high electron conductivity of the porous layer, the proton current conservation equation in the film is

$$\frac{\partial j}{\partial x} = -i_* \left( \frac{c_{Nm}}{c_h^{in}} \right) \exp\left( \frac{\eta}{b} \right) \tag{8}$$

where the right side is the Tafel rate of proton consumption in the ORR. Here,  $c_{Nm}$  is the dissolved oxygen concentration at the Pt surface

$$c_{Nm} \equiv c_N(R_m) \tag{9}$$

where  $R_m$  is the Pt cone radius (Figure 1):

$$R_m(x) = R_p(x) + l_N / \cos \alpha, \tag{10}$$

and  $l_N$  is the ionomer film thickness. With the dimensionless variables, Equation (8) takes the form

$$\varepsilon^2 \frac{\partial \tilde{j}}{\partial \tilde{x}} = -\tilde{c}_{Nm} \exp \tilde{\eta} \tag{11}$$

According to the Ohm's law,  $\tilde{j}=-\partial\tilde{\eta}/\partial\tilde{x}$  and Equation (11) transforms to the diffusion-like equation for the ORR overpotential

$$\varepsilon^2 \frac{\partial^2 \tilde{\eta}}{\partial \tilde{x}^2} = \tilde{c}_{Nm} \exp \tilde{\eta}$$
 (12)

Radial oxygen flux  $N_p$  at the pore/ionomer interface is determined from equation for radial transport of dissolved

Chemistry Europe

European Chemical Societies Publishing

oxygen through the ionomer film:

$$\frac{D_N}{r\cos^2(\alpha)}\frac{\partial}{\partial r}\left(r\frac{\partial c_N}{\partial r}\right)=0,\quad c_N(R_p)=K_Hc(x),$$

$$\left. \frac{D_N}{\cos(\alpha)} \frac{\partial c_N}{\partial r} \right|_{r=R_m} = -\frac{R_p^2 i_*}{2R_m (4F)} \left( \frac{c_N(R_m)}{c_h^{in}} \right) \exp\left(\frac{\eta}{b}\right) \quad (13)$$

where  $K_H$  is the dimensionless Henry's constant for oxygen dissolution in the ionomer. The first boundary condition to Equation (13) describes dissolution of the gaseous oxygen in the Nafion film according to the Henry's law. More complicated effects of oxygen transport through the pore/film and film/metal interface are out of the present model scope. The factors with  $\cos \alpha$  arise as the oxygen diffusion path (concentration gradient) is slanted with respect to the radial direction (Figure 1). The factor  $R_p^2/(2R_m)$  in the right boundary condition for Equation (13) provides correct transition of the model to the standard macrohomogeneous model for oxygen and proton transport in the limit of zero ionomer film thickness [15].

With the dimensionless variables, Equation (13) takes the form

$$\frac{\tilde{D}_{N}}{\tilde{r}} \frac{\partial}{\partial \tilde{r}} \left( \tilde{r} \frac{\partial \tilde{c}_{N}}{\partial \tilde{r}} \right) = 0, \quad \tilde{c}_{N}(\tilde{R}_{p}) = K_{H} \tilde{c}(\tilde{x}),$$

$$\varepsilon^{2} \gamma_{p} \tilde{D}_{N} \frac{\partial \tilde{c}_{N}}{\partial r} \Big|_{\tilde{r} - \tilde{R}} = -\tilde{c}_{N}(\tilde{R}_{m}) e^{\tilde{\eta}} \quad (14)$$

where

$$\gamma_p = \frac{2\tilde{R}_m}{\tilde{R}_p^2 \cos \alpha} \tag{15}$$

Solution to Equation (14) is

$$\tilde{c}_{N}(\tilde{r}) = \frac{\left(\tilde{R}_{p}^{2} \ln{(\tilde{R}_{m}/\tilde{r})}e^{\tilde{\gamma}} + \gamma_{p}\varepsilon^{2}\tilde{D}_{N}\right)K_{H}\tilde{c}}{\left(\tilde{R}_{p}^{2} \ln{(\tilde{R}_{m}/\tilde{R}_{p})}e^{\tilde{\gamma}} + \gamma_{p}\varepsilon^{2}\tilde{D}_{N}\right)}$$
(16)

Setting here  $\tilde{r} = \tilde{R}_m$  we get  $\tilde{c}_{Nm}$  appearing in Equation (12):

$$\tilde{c}_{Nm} = \frac{K_H \tilde{c}}{1 + \xi e^{\tilde{\eta}}} \tag{17}$$

where

$$\xi = \frac{\tilde{R}_p^2 \ln \left( \tilde{R}_m / \tilde{R}_p \right) \cos \alpha}{2\varepsilon^2 \tilde{D}_N}.$$
 (18)

Differentiating (16) over  $\tilde{r}$  and multiplying the result by  $\tilde{D}_N$  we get the oxygen flux  $\tilde{N}_p = -\tilde{D}_N \partial \tilde{c}_N / \partial \tilde{r}|_{\tilde{r} = \tilde{R}_n}$  on the

ionomer side of the pore/ionomer interface:

$$\tilde{N}_p = \frac{\tilde{R}_p \cos(\alpha)}{2\varepsilon^2} \, \tilde{c}_{Nm} e^{\tilde{\eta}}. \tag{19}$$

# 2.3 | Static equations

Using Equation (19) and Equation (17) in Equation (5), we get equation for the oxygen transport in a conoid pore with reactive walls:

$$\varepsilon^2 \tilde{D}_{ox} \left( \frac{\partial^2 \tilde{c}}{\partial \tilde{x}^2} + \frac{2 \tan(\alpha)}{\tilde{R}_p} \frac{\partial \tilde{c}}{\partial \tilde{x}} \right) = \frac{K_H \tilde{c} \, e^{\tilde{\eta}}}{1 + \xi e^{\tilde{\eta}}}$$
 (20)

Using Equation (17) in (12) we come to equation for the overpotential

$$\varepsilon^2 \frac{\partial^2 \tilde{\eta}}{\partial \tilde{x}^2} = \frac{K_H \tilde{c} \, e^{\tilde{\eta}}}{1 + \xi e^{\tilde{\eta}}} \tag{21}$$

The system of equations (20) and (21) describes the shapes  $\tilde{c}(\tilde{x})$  and  $\tilde{\eta}(\tilde{x})$  along the pore. The boundary conditions for this system are quite obvious

$$\frac{\partial \tilde{c}}{\partial \tilde{x}}\Big|_{\tilde{x}=0} = 0, \quad \tilde{c}(1) = \tilde{c}_1, 
\frac{\partial \tilde{\eta}}{\partial \tilde{x}}\Big|_{\tilde{x}=0} = -\tilde{j}_0, \quad \frac{\partial \tilde{\eta}}{\partial \tilde{x}}\Big|_{\tilde{x}=1} = 0 \quad (22)$$

where  $\tilde{c}_1$  ic the oxygen concentration at the pore/GDL interface, and  $\tilde{j}_0$  is the cell current density.

#### 3 | PORE IMPEDANCE

# 3.1 | Transient transport equations

The transient versions of Equations (21) and (20) are

$$\frac{\partial \tilde{\eta}}{\partial \tilde{t}} - \varepsilon^2 \frac{\partial^2 \tilde{\eta}}{\partial \tilde{x}^2} = -\tilde{c}_{Nm} e^{\tilde{\eta}}$$
 (23)

$$\mu^2 \frac{\partial \tilde{c}}{\partial \tilde{t}} - \varepsilon^2 \tilde{D}_{ox} \left( \frac{\partial^2 \tilde{c}}{\partial \tilde{x}^2} + \frac{2 \tan(\alpha)}{\tilde{R}_p} \frac{\partial \tilde{c}}{\partial \tilde{x}} \right) = -\frac{2\varepsilon^2 \tilde{N}_p}{\tilde{R}_p \cos \alpha}$$
 (24)

where  $\mu$  is the constant parameter

$$\mu = \sqrt{\frac{4Fc_h^{in}}{C_{dl}b}}. (25)$$

The system of Equations (23) and (24) describes the transient shapes  $\tilde{\eta}(\tilde{t}, \tilde{x})$ ,  $\tilde{c}(\tilde{t}, \tilde{x})$  along the pore. The boundary conditions for this system are given by Equations (22).



Linearization and Fourier–transform of Equations (23) and (24) lead to the linear equations for the small perturbation amplitudes  $\tilde{\eta}^1$  and  $\tilde{c}^1$  in the  $\tilde{\omega}$ –space:

$$\mathrm{i}\tilde{\omega}\tilde{\eta}^{1}-\varepsilon^{2}\frac{\partial^{2}\tilde{\eta}^{1}}{\partial\tilde{x}^{2}}=-\mathrm{e}^{\tilde{\eta}^{0}}\tilde{c}_{Nm}^{1}-\tilde{c}_{Nm}^{0}\mathrm{e}^{\tilde{\eta}^{0}}\tilde{\eta}^{1} \qquad (26)$$

$$i\tilde{\omega}\mu^{2}\tilde{c}^{1} - \varepsilon^{2}\tilde{D}_{ox}\left(\frac{\partial^{2}\tilde{c}^{1}}{\partial\tilde{x}^{2}} + \frac{2\tan(\alpha)}{\tilde{R}_{p}}\frac{\partial\tilde{c}^{1}}{\partial\tilde{x}}\right) = -\frac{2\varepsilon^{2}\tilde{N}_{p}^{1}}{\tilde{R}_{p}\cos\alpha}$$
(27)

where

$$\tilde{N}_{p}^{1} = -\tilde{D}_{N} \frac{\partial \tilde{c}_{N}^{1}}{\partial \tilde{r}} \bigg|_{\tilde{r} = \tilde{R}_{p}}$$
(28)

is the dissolved oxygen flux perturbation amplitude at the pore/ionomer interface.

Parameter  $\tilde{c}_{Nm}^0$  is given by Equation (17), while  $\tilde{c}_{Nm}^1$  and  $\tilde{N}_p^1$  result from the problem for dissolved oxygen transport through the Nafion film. The latter is an obvious transient extension of Equation (14):

$$\mu^{2} \frac{\partial \tilde{c}_{N}}{\partial \tilde{t}} - \frac{\varepsilon^{2} \tilde{D}_{N}}{\tilde{r}} \frac{\partial}{\partial \tilde{r}} \left( \tilde{r} \frac{\partial \tilde{c}_{N}}{\partial \tilde{r}} \right) = 0,$$

$$\tilde{c}_{N}(\tilde{R}_{p}) = K_{H} \tilde{c}(\tilde{x}), \quad \gamma_{p} \varepsilon^{2} \tilde{D}_{N} \frac{\partial \tilde{c}_{N}}{\partial \tilde{r}} \Big|_{\tilde{r} = \tilde{R}_{m}} = -\tilde{c}_{Nm} e^{\tilde{\eta}}$$
(29)

Linearization and Fourier–transform of Equation (29) give equation for the perturbation amplitude  $\tilde{c}_N^1$ :

$$\begin{split} \mathrm{i}\tilde{\omega}\mu^{2}\tilde{c}_{N}^{1} - \frac{\varepsilon^{2}\tilde{D}_{N}}{\tilde{r}} \frac{\partial}{\partial\tilde{r}} \left( \tilde{r} \frac{\partial\tilde{c}_{N}^{1}}{\partial\tilde{r}} \right) &= 0, \\ \tilde{c}_{N}^{1}(\tilde{R}_{p}) &= K_{H}\tilde{c}^{1}(\tilde{x}), \end{split} \tag{30}$$
 
$$\gamma_{p}\varepsilon^{2}\tilde{D}_{N} \frac{\partial\tilde{c}_{N}^{1}}{\partial\tilde{r}} \bigg|_{\tilde{r}=\tilde{R}_{m}} &= -\mathrm{e}^{\tilde{\eta}^{0}}\tilde{c}_{Nm}^{1} - \tilde{c}_{Nm}^{0}\mathrm{e}^{\tilde{\eta}^{0}}\tilde{\eta}^{1} \end{split}$$

Solution to the linear Equation (30) allows us to calculate parameters appearing in Equations (26) and (27):

$$\tilde{c}_{Nm}^1 = \frac{A_c}{B_c} \tilde{c}^1 + \frac{A_{\eta}}{B_c} \tilde{\eta}^1,$$

$$\tilde{N}_p^1 = \tilde{D}_N \left( \frac{Q_c}{B_c} \tilde{c}^1 + \frac{Q_{\eta}}{B_c} \tilde{\eta}^1 \right) \quad (31)$$

where the coefficients  $A_c$ ,  $A_{\eta}$ ,  $B_c$ ,  $Q_c$ ,  $Q_{\eta}$  and  $B_N$  are given in Appendix.

Using Equations (31) in Equations (26) and (27), we come to the system

$$\frac{\partial^2 \tilde{\eta}^1}{\partial \tilde{x}^2} = p\tilde{c}^1 + q\tilde{\eta}^1, \quad \tilde{\eta}^1(1) = \tilde{\eta}^1_1, \quad \frac{\partial \tilde{\eta}^1}{\partial \tilde{x}} \bigg|_{\tilde{x}=1} = 0 \quad (32)$$

$$\left.\frac{\partial^2 \tilde{c}^1}{\partial \tilde{x}^2} + u \frac{\partial \tilde{c}^1}{\partial \tilde{x}} = k \tilde{c}^1 + s \tilde{\eta}^1, \quad \left.\frac{\partial \tilde{c}^1}{\partial \tilde{x}}\right|_{\tilde{x}=0} = 0, \quad \tilde{c}^1(1) = \tilde{c}^1_1$$

(33)

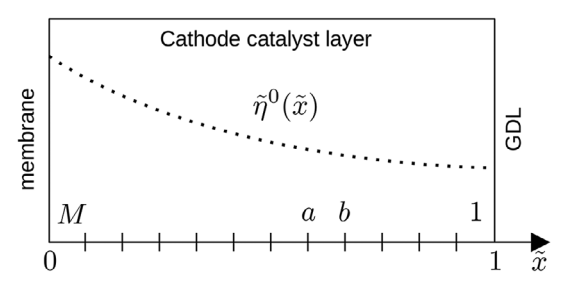


FIGURE 2 A uniform computational grid with M cells for impedance calculations. Note that the cells [a, b] are numbered from the GDL to the membrane.

where the coefficient functions are given by

$$p = \frac{e^{\tilde{\eta}^{0}} A_{c}}{\varepsilon^{2} B_{c}}, \quad q = \frac{1}{\varepsilon^{2}} \left( \frac{e^{\tilde{\eta}^{0}} A_{\eta}}{B_{c}} + \tilde{c}_{Nm}^{0} e^{\tilde{\eta}^{0}} + i\tilde{\omega} \right),$$

$$k = \frac{2\tilde{D}_{N}}{\tilde{D}_{ox} \tilde{R}_{p} \cos \alpha} \frac{Q_{c}}{B_{c}} + \frac{i\tilde{\omega}\mu^{2}}{\varepsilon^{2} \tilde{D}_{ox}},$$

$$s = \frac{2\tilde{D}_{N}}{\tilde{D}_{ox} \tilde{R}_{p} \cos \alpha} \frac{Q_{\eta}}{B_{c}}, \quad u = \frac{2\tan(\alpha)}{\tilde{R}_{p}} \quad (34)$$

# 3.2 | Numerical method

The system (32), (33) is a boundary–value problem with variable coefficients. Analytical solution of the system is hardly possible even in the case of  $\tilde{x}$ –independent coefficients p,q,k,s,u. Numerical solution can be obtained using the following idea.

We introduce a uniform computational grid on the interval [0,1] and formulate a Cauchy problem for Equations (32) and (33) on a single numerical cell  $\tilde{x} \in [a,b]$ , with the following boundary conditions at  $\tilde{x} = b$  (Figure 2):

$$\tilde{\eta}^{1}(b) = \tilde{\eta}_{b}^{1}, \quad \frac{\partial \tilde{\eta}^{1}}{\partial \tilde{x}} \bigg|_{\tilde{x}=b} = -\tilde{J}_{b}^{1}, 
\tilde{c}^{1}(b) = \tilde{c}_{b}^{1}, \quad \frac{\partial \tilde{c}^{1}}{\partial \tilde{x}} \bigg|_{\tilde{x}=b} = \tilde{N}_{b}^{1}$$
(35)

where the subscript b indicates the values at  $\tilde{x} = b$ . Approximate solution of Equations (32), (33), and (35) in the vicinity of  $\tilde{x} = b$  in the form of Taylor series is

$$\begin{split} \tilde{\eta}^1 &\simeq \tilde{\eta}_b^1 + \tilde{j}_b^1(b - \tilde{x}) + \frac{1}{2} \Big( p \tilde{c}_b^1 - q \tilde{\eta}_b^1 \Big) (b - \tilde{x})^2 \\ &\qquad \qquad - \frac{1}{6} \Big( p \tilde{N}_b^1 - q \tilde{j}_b^1 \Big) (b - \tilde{x})^3 \end{split} \tag{36}$$

$$\tilde{c}^{1} \simeq \tilde{c}_{b}^{1} - \tilde{N}_{b}^{1}(b - \tilde{x}) + \frac{1}{2} \left( s \tilde{\eta}_{b}^{1} + k \tilde{c}_{b}^{1} - u \tilde{N}_{b}^{1} \right) (b - \tilde{x})^{2}$$

$$- \frac{1}{6} \left( (u^{2} + k) \tilde{N}_{b}^{1} - u \left( s \tilde{\eta}_{b}^{1} + k \tilde{c}_{b}^{1} \right) - s \tilde{j}_{b}^{1} \right) (b - \tilde{x})^{3}$$
 (37)

where the four leading terms are kept.

Calculating the derivatives  $\tilde{J}_a^1 = -\partial \tilde{\eta}^1/\partial \tilde{x}|_{\tilde{x}=a}$ ,  $\tilde{N}_a^1 = \partial \tilde{c}^1/\partial \tilde{x}|_{\tilde{x}=a}$  and setting  $\tilde{x}=a$  in Equations (36) and (37), we get expressions of the unknown functions at  $\tilde{x}=a$  through their values at  $\tilde{x}=b$ :

$$\tilde{\eta}_{a}^{1} = \tilde{\eta}_{b}^{1} + \tilde{J}_{b}^{1}\tilde{l} + \frac{y_{1}\tilde{l}^{2}}{2} + \frac{y_{2}\tilde{l}^{3}}{6}$$

$$\tilde{J}_{a}^{1} = \tilde{J}_{b}^{1} + y_{1}\tilde{l} + \frac{y_{2}\tilde{l}^{2}}{2}$$

$$\tilde{c}_{1}^{1} = \tilde{c}_{b}^{1} - \tilde{N}_{b}^{1}\tilde{l} + \frac{y_{3}\tilde{l}^{2}}{2} + \frac{y_{4}\tilde{l}^{3}}{6}$$

$$\tilde{N}_{a}^{1} = \tilde{N}_{b}^{1} - y_{3}\tilde{l} - \frac{y_{4}\tilde{l}^{2}}{2}$$
(38)

where  $\tilde{l} = b - a$  is the computational cell length, and

$$\begin{aligned} y_1 &= p\tilde{c}_b^1 + q\tilde{\eta}_b^1, \quad y_2 &= -p\tilde{N}_b^1 + q\tilde{j}_b^1, \\ y_3 &= k\tilde{c}_b^1 + s\tilde{\eta}_b^1 - u\tilde{N}_b^1, \\ y_4 &= -(u^2 + k)\tilde{N}_b^1 + u\left(k\tilde{c}_b^1 + s\tilde{\eta}_b^1\right) + s\tilde{j}_b^1. \end{aligned} \tag{39}$$

The coefficient functions p, q, k, s, u in Equations (39) are calculated at the cell center  $\tilde{x} = (b + a)/2$ .

Equations (38) are the recurrent relations; to obtain the unknown functions at all grid points, the values at  $\tilde{x}=1$  have to be specified. For simplicity, we consider the case of fast oxygen transport in the channel and GDL, meaning that  $\tilde{c}_1^1=0$ :

$$\tilde{\eta}_b^1 = \tilde{\eta}_1^1, \quad \tilde{c}_b^1 = 0, \quad \tilde{j}_b^1 = 0, \quad \tilde{N}_b^1 = \tilde{N}_1^1$$
 (40)

Here,  $\tilde{\eta}_1^1$  is the applied potential perturbation and  $\tilde{N}_1^1$  is yet undefined parameter. The parameter  $\tilde{N}_1^1$ , is a solution to equation

$$\tilde{N}_0^1 \left( \tilde{N}_1^1 \right) = 0 \tag{41}$$

meaning that the oxygen flux perturbation  $\tilde{N}_0^1$  at the membrane must be zero. Solution of this equation is discussed below.

With  $\tilde{N}_1^1$  at hand, we can iterate Equations (38) M times, setting after each iteration

$$\tilde{\eta}_{b}^{1} = \tilde{\eta}_{a}^{1}, \quad \tilde{j}_{b}^{1} = \tilde{j}_{a}^{1}, \quad \tilde{c}_{b}^{1} = \tilde{c}_{a}^{1}, \quad \tilde{N}_{b}^{1} = \tilde{N}_{a}^{1},$$
 (42)

where M is the number of cells (Figure 2). This procedure gives us solution at all the grid points. The values  $\tilde{\eta}_0^1$  and  $\tilde{j}_0^1$ 

TABLE 1 Pore/cell geometrical and operating parameters.

. 0	01
Pore length $l_t$ , cm	$3 \times 10^{-4} (3 \mu\text{m})$
Mean pore radius, $R_p$ , nm	32.2
Pore angle $\alpha$ , rad	$(\pi/4) \times 1.08 \times 10^{-2}$
Nafion film thickness $l_N$ , cm	10 <sup>-6</sup> (10 nm)
ORR exchange current density, $i_*$ , A cm <sup>-3</sup>	$10^{-3}$
Henry's constant for oxygen solubility	
in water at 80°C, mol/mol	$6.76 \times 10^{-3}$
ORR Tafel slope b / V (per exponent)	0.03
Ionomer proton conductivity, $\sigma_N$ / mS cm <sup>-2</sup>	<sup>-1</sup> 1
Double layer capacitance $C_{dl}$ / F cm <sup>-3</sup>	20
Cell current density $j_0$ / A cm <sup>-2</sup>	0.5
Relative humidity	50%
Cathode absolute pressure, kPa	150
Cell temperature, K	273 + 80

at the membrane interface lead to the pore impedance

$$\tilde{Z} = \frac{\tilde{\eta}_0^1}{\tilde{j}_0^1}.\tag{43}$$

Numerical method based on Equation (38) is at least an order of magnitude faster than the standard BVP solver (see below).

# 4 | RESULTS AND DISCUSSION

### 4.1 | Static shapes

It is interesting to compare performance of conical and cylindrical pores with the same side surface (electrochemically active) area. The pore length taken for the calculations is 3  $\mu$ m, a typical thickness of low–Pt electrodes with the Pt loading of about 0.1 mg cm<sup>-2</sup>. The other parameters for the calculations are listed in Table 1.

The mean radius of the conical pore and the radius of equivalent cylindrical pore were taken to be 32 nm, which is the mean pore radius of a standard Pt/C electrode from Gore [18]. The angle of conical pore is taken to provide the pore radius at the GDL interface twice larger than the pore radius at the membrane. This leads to a small angle of  $\alpha \simeq R_p/l_t \simeq 0.0107$  rad, or 0.615 degrees, which allows us to set  $\cos(alpha) = 1$ . The other parameters are listed in Table 1.

Equations (20) and (21) have been solved using Python boundary–value solver *solve\_bvp*. The oxygen concentration and overpotential shapes in the conical and cylindrical pores are compared in Figure 3. In the range of  $0.2 \le \tilde{x} \le 1$ , the oxygen concentration shape in the conical pore is close to linear indicating a more uniform rate of oxygen consumption along the pore (Figure 3). The gain in the cell

ch Center, Wiley Online Library on [23/08/2024]. See the Terms

on Wiley Online Library for rules

use; OA articles are governed by the applicable Creative Commons License

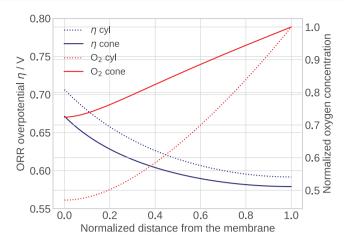


**FIGURE 3** The shapes of oxygen concentration and ORR overpotential  $\eta$  along the conical and cylindrical pores. The cell current density is 1.0 A cm<sup>-2</sup>.

potential is equal to the difference of overpotentials at  $\tilde{x} = 0$ ; this gain is about 50 mV (Figure 3). Note that the gain increases with the growth of the pore angle  $\alpha$  (see below).

# 4.2 | Impedance

Equation (41) has been solved using Python *fsolve* routine and the same system of recurrent Equations (38) and (39). Note that  $\tilde{N}_1^1$  is a complex–valued parameter and for using *fsolve*, Equation (41) should be formulated as a system of two equations, for the real and imaginary parts of  $\tilde{N}_1^1$ . A good initial guess is  $\{\Re(\tilde{N}_1^1),\Im(\tilde{N}_1^1)\}=\{\tilde{\eta}_1^1,\tilde{\eta}_1^1\}$ .

The conical pore impedance for the parameters in Table 1 calculated using Equations (38) on a grid with M=30 cells is shown in Figure 4. For comparison, the same impedance calculated from the system of Equations (32), (33) using the standard Python BVP solver  $solve\_bvp$  is also shown. As can be seen, the results are almost identical; however, in this case the method of recurrent equations (38) is about 20 times faster than the standard BVP solver.

Figure 5 shows the impedance spectrum of the equivalent cylindrical pore for the same set of parameters (Table 1). Comparison of the Nyquist spectra in Figures 5a and 4a immediately shows superior performance of the conical pore. It is interesting to note that the peak of  $-\Im(Z)$  of the conical pore impedance is shifted toward a higher frequency as compared to this peak position of the cylindrical pore impedance (cf. Figures 5b and 4b). Distribution of relaxation times (DRT) spectra show that the peaks of the conical pore impedance exhibit quite significant shift toward higher frequencies (to be published elsewhere).

The positive effect of pore conical shape on the performance exists for any mean pore radius. Figure 6 shows that

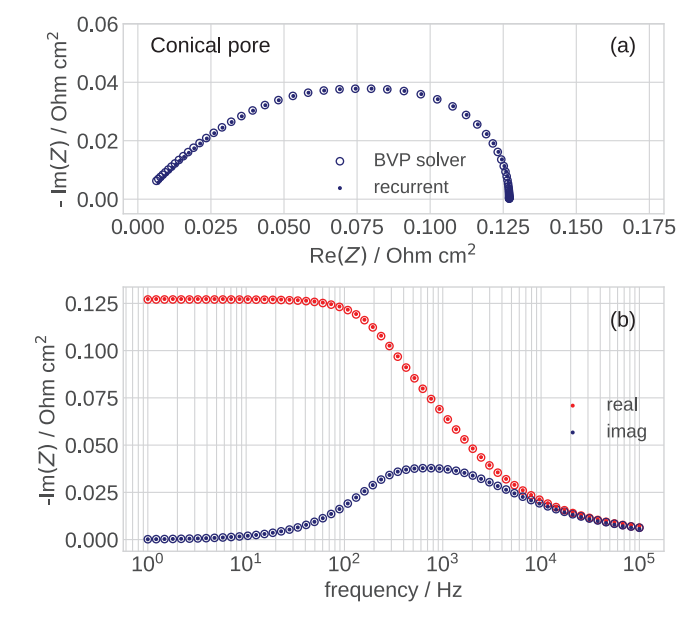


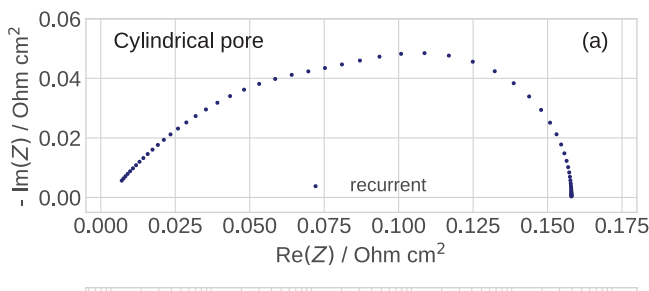
FIGURE 4 (a) The Nyquist spectra of the conical pore calculated with the recurrent Equations (38) on the grid with 30 cells (points) and from the direct numerical solution of Equations (32), (33) using the standard Python BVP solver (open circles). (b) The frequency dependencies of the real and imaginary parts of the spectra in (a).

the potential loss (the ORR overpotential at the membrane interface) decreases linearly with the growth of the pore half–angle  $\alpha$ .

At the present state of technology, it seems that making the CCL with conical pores of the mean radius about several tens of nanometers is hardly feasible. Ideally, it would be great to produce a regular "grid" of nanopores converging toward the membrane. To the best of the author's knowledge, conical pores could be designed using poreformers. However, this technique could produce pores of a radius of about 0.1–1  $\mu$ m. One cannot make pores with one to two orders of magnitude smaller radius in this way. However, this work demonstrates possible direction for further development of highly efficient CCL for low–Pt PEMFCs.

#### 5 | CONCLUSIONS

A model for transient electrochemical performance of a conical pore in a low-Pt cathode catalyst layer is developed. An equation for diffusive oxygen transport along the conical pore is derived. This equation is coupled to the proton transport and dissolved oxygen transport equations in a thin ionomer film separating open pore from the coaxial Pt surface. Numerical solution of the steady-state equations shows that already at a very small conoid angle, the conoid nanopore performance quite



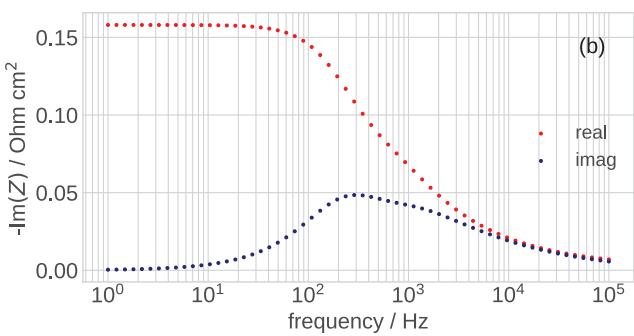


**FIGURE 5** (a) The Nyquist spectra of the cylindrical pore calculated with the recurrent Equations (38) on the grid with 30 cells (points). (b) The frequency dependence of the real and imaginary parts of the spectrum in (a).

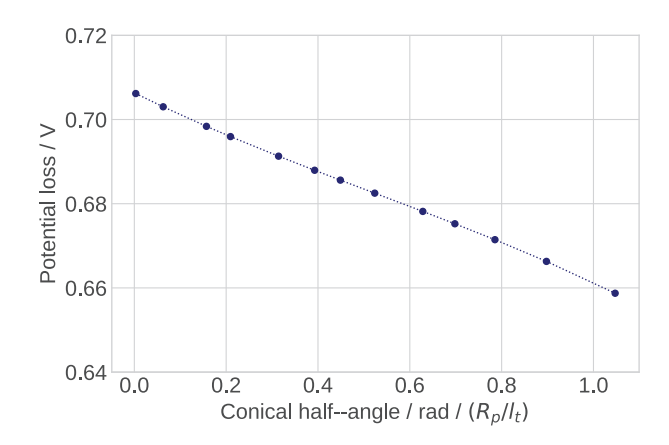


**FIGURE 6** Total potential loss vs the conoid half–angle for the conical pore calculated with the data in Table 1 and the cell current density of 1 A cm<sup>-2</sup>. The range of  $\alpha$  shown in this plot is equivalent to 0 (cylindrical pore) to  $1.13 \times 10^{-2}$  rad.

significantly exceeds the performance of a cylindrical pore with the equivalent active surface area. Further, equations for small–amplitude AC perturbations of oxygen concentration and overpotential in the pore are derived. A fast method for solution of this system of linear ODEs is developed and used for calculation of the pore impedance. Comparison with the cylindrical pore impedance shows a shift of the conical pore spectrum features toward higher frequencies.

# **NOMENCLATURE**

- ~ Marks dimensionless variables
- b ORR Tafel slope, V
- $C_{dl}$  Double layer volumetric capacitance, F cm<sup>-3</sup>
  - C Oxygen molar concentration in the pore, mol cm<sup>-3</sup>
- $c_N$  Dissolved oxygen molar concentration in the ionomer, mol cm<sup>-3</sup>
- $c_h^{in}$  Reference (inlet) oxygen concentration, mol cm<sup>-3</sup>
- $D_{ox}$  Oxygen diffusion coefficient in the pore, cm<sup>2</sup>
- $D_N$  Oxygen diffusion coefficient in the ionomer, cm<sup>2</sup> s<sup>-1</sup>
  - E Dimensionless parameter, Equation (A6)
- F Faraday constant, C mol<sup>-1</sup>
- $J_0, J_1$  Bessel functions of the first kind
  - $i_*$  ORR volumetric exchange current density, A cm<sup>-3</sup>
  - i Imaginary unit
  - J Mean current density in the cell, A cm $^{-2}$
  - j Local proton current density in the film, A cm<sup>-2</sup>
- $K_H$  Dimensionless Henry's constant for oxygen dissolution in the ionomer, mol/mol
- $K_0, K_1$  Modified Bessel functions of the second kind
  - *l* Length of the computational cell,  $\tilde{l} = b a$
  - $l_t$  Pore length, cm
  - M Number of computational cells
  - $N_p$  Oxygen diffusive flux at the pore/ionomer interface, mol cm<sup>-2</sup> s<sup>-1</sup>
- p, q, k, s, u Coefficients in equations, Equation (34)
  - $R_n$  Pore radius, cm
  - $R_m$  Pt/C radius, cm
  - r Radial coordinate, cm
  - t Time, s
  - x Coordinate along the pore, cm
  - Z Impedance  $\Omega$  cm<sup>2</sup>

# **Subscripts**

- 0 Membrane/pore interface
- 1 Pore/GDL interface
- a, b  $\tilde{x}$ -coordinates of a computational cell
- N Ionomer film

# **Superscripts**

- 0 Steady-state value
- 1 Small-amplitude perturbation

### Greek

- $\alpha$  Cone half-angle, rad
- $\gamma_n$  Dimensionless parameter, Equation (15)
- $\eta$  ORR overpotential, positive by convention, V
- $\varepsilon$  Dimensionless parameter, Equation (6)
- $\mu$  Dimensionless parameter, Equation (25)
- $\sigma_N$  Ionomer film proton conductivity, S cm<sup>-1</sup>
  - $\xi$  Dimensionless parameter, Equation (18)
- $\phi, \psi$  Dimensionless parameters, Equation (A6)
  - $\omega$  Angular frequency of the AC signal, s<sup>-1</sup>

#### CONFLICT OF INTEREST STATEMENT

The author declares no conflict of interest.

### DATA AVAILABILITY STATEMENT

No data has been generated in this research.

#### ORCID

Andrei Kulikovsky https://orcid.org/0000-0003-1319-576X

#### REFERENCES

- Y. Sun, S. Polani, F. Luo, S. Ott, P. Strasser, F. Dionigi, *Nature Comm.* 2021, 12, 5984.
- X. Deng, J. Zhang, Z. Fan, W. Tan, G. Yang, W. Wang, W. Zhou, Z. Shao, Energy Fuels 2020, 34, 9175.
- 3. Y. Liu, M. W. Murphy, D. R. Baker, W. Gu, C. Ji, J. Jorne, H. A. Gasteiger, *J. Electrochem. Soc.* **2009**, *156*, B970.
- Y. Liu, C. Li, W. Gu, J. Jorne, H. A. Gasteiger, J. Electrochem. Soc. 2011, 158, B614.
- A. Ohma, T. Mashio, K. Sato, H. Iden, Y. Ono, K. Sakai, K. Akizuki, S. Takaichi, K. Shinohara, *Electrochim Acta* 2011, 56, 10832.
- 6. T. Suzuki, K. Kudo, Y. Morimoto, J. Power Sources 2013, 222, 379.
- T. Suzuki, H. Yamada, K. Tsusaka, Y. Morimoto, J. Electrochem. Soc. 2018, 165, F166.
- 8. T. Mashio, H. Idena, A. Ohma, T. Tokumasu, *J. Electroanal. Chem.* **2017**, 790, 27.
- 9. R. Darling, J. Electrochem. Soc. 2019, 166, F3058.
- 10. R. Darling, S. F. Burlatsky, J. Electrochem. Soc. 2020, 167, 104506.
- M. Moore, S. Shukla, S. Voss, K. Karan, I. Zenyuk, M. Secanell, J. Electrochem. Soc. 2021, 168, 044519.
- 12. M. Atwa, X. Li, Z. Wang, S. Dull, S. Xu, X. Tong, R. Tang, H. Nishihara, F. Prinz, V. Birss, *Mater. Horiz.* **2021**, *8*, 2451.
- J. Liu, S. Liu, F. Yan, Z. Wen, W. Chen, X. Liu, Q. Liu, J. Shang,
   R. Yu, D. Su, J. Shui, J. Am. Chem. Soc. 2022, 144, 19106.
- 14. A. Z. Weber, A. Kusoglu, J. Mater. Chem. A 2014, 2, 17207.
- 15. A. Kulikovsky, Electrochem. Comm. 2019, 103, 61.

- 16. T. Reshetenko, A. Kulikovsky, RSC Adv. 2019, 9, 38797.
- E. Sadeghi, A. Putz, M. Eikerling, J. Electrochem. Soc. 2013, 160, F1159.
- 18. H. Yu, L. Bonville, R. Maric, J. Electrochem. Soc. 2018, 165, F272.

How to cite this article: A. Kulikovsky, *Electrochem. Sci. Adv.* **2024**, *4*, e202300006. https://doi.org/10.1002/elsa.202300006

# APPENDIX: COEFFICIENTS IN EQUATIONS (31), (34)

$$A_c = (iK_1(-i\phi\tilde{R}_m)J_0(\phi\tilde{R}_m) + K_0(-i\phi\tilde{R}_m)J_1(\phi\tilde{R}_m))\phi K_H$$
(A1)

$$A_{\eta} = \left(J_{0}(\phi\tilde{R}_{m})K_{0}\left(-\mathrm{i}\phi\tilde{R}_{p}\right) - J_{0}\left(\phi\tilde{R}_{p}\right)K_{0}(-\mathrm{i}\phi\tilde{R}_{m})\right)E\tilde{c}_{Nm}^{0} \tag{A2} \label{eq:Aeta}$$

$$B_{c} = \left(iK_{1}(-i\phi\tilde{R}_{m})J_{0}(\phi\tilde{R}_{p}) + K_{0}(-i\phi\tilde{R}_{p})J_{1}(\phi\tilde{R}_{m})\right)\phi$$

$$+ \left(J_{0}(\phi\tilde{R}_{p})K_{0}(-i\phi\tilde{R}_{m}) - J_{0}(\phi\tilde{R}_{m})K_{0}(-i\phi\tilde{R}_{p})\right)E$$
(A3)

$$Q_{c} = K_{H} \left( J_{1} \left( \phi \tilde{R}_{p} \right) K_{1} (-i \phi \tilde{R}_{m}) - J_{1} (\phi \tilde{R}_{m}) K_{1} \left( -i \phi \tilde{R}_{p} \right) \right) \psi$$

$$+ K_{H} \left( i J_{0} (\phi \tilde{R}_{m}) K_{1} \left( -i \phi \tilde{R}_{p} \right) + J_{1} \left( \phi \tilde{R}_{p} \right) K_{0} (-i \phi \tilde{R}_{m}) \right) E \phi$$
(A4)

$$Q_{\eta} = \left(iJ_{0}\left(\phi\tilde{R}_{p}\right)K_{1}\left(-i\phi\tilde{R}_{p}\right) + K_{0}\left(-i\phi\tilde{R}_{p}\right)J_{1}\left(\phi\tilde{R}_{p}\right)\right)\phi E\tilde{c}_{Nm}^{0}$$
(A5)

where  $J_0$ ,  $J_1$  are the Bessel functions of the first kind and  $K_0$ ,  $K_1$  are the modified Bessel functions of the second kind. Further,

$$E = \frac{e^{\tilde{\eta}^0}}{\gamma_p \varepsilon^2 \tilde{D}_N}, \quad \psi = \frac{\tilde{\omega} \mu^2}{\varepsilon^2 \tilde{D}_N}, \quad \gamma_p = \frac{2\tilde{R}_m}{\tilde{R}_p^2 \cos \alpha}, \quad (A6)$$
$$\phi = \sqrt{-i\psi},$$

and

$$\tilde{c}_{Nm}^{0} = \frac{K_{H}\tilde{c}^{0}}{1 + \xi e^{\tilde{\eta}^{0}}}, \quad \xi = \frac{\tilde{R}_{p}^{2} \ln \left(\tilde{R}_{m}/\tilde{R}_{p}\right) \cos \alpha}{2\varepsilon^{2} \tilde{D}_{N}}. \quad (A7)$$